ISSN 2411-3336; e-ISSN 2541-9404

JOURNAL OF MINING INSTITUTE

Zapiski Gornogo instituta

Journal homepage: pmi.spmi.ru

Research article *Geology*

Olivine potential for water transport to the mantle under warm and hot subduction conditions

Igor N. Kupriyanov✉, Aleksandr G. Sokol
V.S.Sobolev Institute of Geology and Mineralogy SB RAS, Novosibirsk, Russia

***How to cite this article*:** Kupriyanov I.N., Sokol A.G. Olivine potential for water transport to the mantle under warm and hot subduction conditions. Journal of Mining Institute. 2026. Vol. 279, p. 3-12.

Abstract
This study experimentally investigates the patterns of hydrogenation of olivine crystals by an aqueous fluid in equilibrium with olivine and orthopyroxene at a pressure of 5.5 GPa and temperatures of 850, 940, 1030, and 1100 °C. It is shown that at *P-T* parameters characteristic of slabs and the portion of the mantle wedge mechanically coupled to slabs under the thermal regimes of warm and hot subduction, the interaction of the aqueous fluid with olivine is largely controlled by the concentration of pre-existing silicon vacancies in olivine crystal structure. As a result, at a temperature of 850 °C, the concentration of OH defects related to Si vacancies increases noticeably relative to the initial value; however, calculated as H_2O, it does not exceed 110 ppm. At 1030 °C, no new Si vacancies are formed, and the water content in olivine remains at the same level as after experiments at lower temperatures. The formation of Si vacancies and their protonation during olivine recrystallization in an aqueous fluid are recorded only at 1100 °C, near the peridotite solidus. In newly formed olivine, the water content reaches 350 ppm. It has been established that an increase in oxygen fugacity from the values of the Ni-NiO (NNO) buffer to those of the Fe_2O_3-Fe_3O_4 (HM) buffer, as well as an increase in NaCl concentration in the fluid from 0 to 9 wt.%, have little or no effect on the solubility of water in olivine. It is concluded that due to the low solubility of water in olivine immediately following the complete dehydration of serpentinized peridotites at depths of ~150-200 km, the efficiency of water transport into the mantle by slabs under the thermal regimes of warm and hot subduction must decrease sharply. Under such conditions, a significant volume of aqueous fluid is released within the slabs, which can participate in the generation of deep magmas and mantle metasomatism.

Keywords
subduction zone; slab; mantle wedge; oceanic crust; serpentine; fluid; nominally anhydrous minerals

Funding
The experiments on the protonation of existing and new vacancies in olivine were carried out under the State assignment of IGM SB RAS (FWZN-2026-0013). The series of experiments with NaCl addition and under buffer controlled redox conditions were supported by the Russian Science Foundation (Project 22-17-00005).

Received: 19.06.2025 ***Accepted: 09.12.2025*** ***Online: 23.04.2026*** ***Published: 20.07.2026***

Introduction

Subduction of oceanic crust and lithosphere is a basic mechanism maintaining a water flux up to 10^{15} g/year from the exosphere to the mantle [1-4]. Most of water is carried by hydrous and nominally anhydrous minerals which are stable at the *P-T* conditions of subduction zones [3, 4]. The features of the temperature patterns and fractionation of alkalis indicate that amphibole and phengite are less efficient water carriers to depths below 120 km than antigorite (high-pressure modification of serpentine) and nominally anhydrous minerals [4, 5]. Serpentine forms in hydrothermal reactions of rocks with sea water percolating through faulted crust and lithosphere [6, 7]. According to geophysical data, the upper lithosphere (< 10 km below the Moho) contains < 4 to 20 % of serpentine which is equivalent to < 0.5 to 2.5 wt.% H_2O [6].

In cold slabs, temperatures do not exceed the stability limits of water-bearing phases [1, 8]. This is clearly seen from the position of the Moho boundary for such slabs, as shown in Fig.1, *a*. In this case, the primary transporters of water into the mantle remain the water-bearing phases – chlorite and

This is an open access article under the CC BY 4.0 license

serpentine, followed by the 10 Å phase [9]. Upon further subduction in cold slabs, down to the mantle transition zone, water can be transported by successive high-pressure water-bearing phases – A → → E → B [3]. Wadsleyite and ringwoodite, which are stable in the transition zone, can contain up to 1-2 wt.% H_2O [10]. The mantle transition zone acts as a global water reservoir and a crucial link in the deep water cycle. Water-enriched material from the transition zone may participate in the generation of komatiitic magmas [11] and agents of upper mantle metasomatism [12], as well as serving as a medium for diamond crystallization [13].

For slabs subducting at hotter temperatures, the stability of antigorite is limited to pressures ranging from ~3 to ~6 GPa, which is equivalent to depths of 100-200 km (Fig.1, *a*, *b*) [5, 14-17]. According to experimental data, at higher pressures there are no stable water-bearing phases capable of replacing serpentine in the peridotite-H_2O system [3-5]. It is traditionally considered that nominally anhydrous minerals can make a significant contribution to the subduction of water into the mantle [4, 18]. Researchers estimate [4], that at pressures of 3-4 GPa and temperatures of 800-1000 °C, nominally anhydrous minerals in subducting peridotite (60 % olivine and 40 % aluminous orthopyroxene) may contain 1400-2900 ppm H_2O. Under these *P-T* conditions, the majority of water will be hosted in orthopyroxene [19]. However, at $P > 5$ GPa, the solubility of water in orthopyroxene drops sharply due to the decrease in aluminum content [20]. To determine the efficiency of water transport by slabs, systematic data are lacking regarding the specifics of water uptake by olivine formed during antigorite dehydration, as well as during the protonation of preexisting silicon [Si] and magnesium [Mg] vacancies in peridotitic olivine. The conclusions of [18] require experimental verification. Based on experimental data obtained over a limited range of *P-T* conditions and a semi-empirical model constructed on that basis, the authors of [18] hypothesized that maximum water concentrations in olivine, ranging from 400 to 2000 ppm, could arise in a layer of the mantle wedge heated to 1100 °C and dragged into the mantle by the slab.

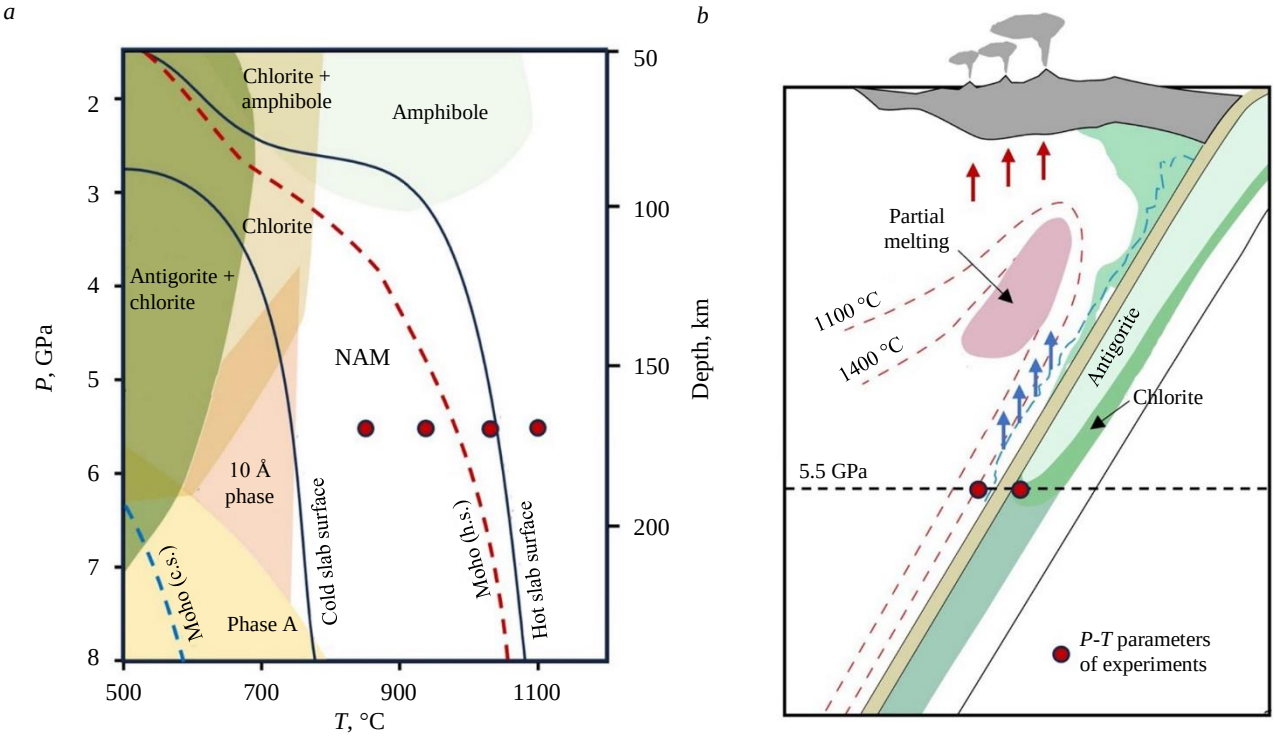


Fig.1. Peridotite-H_2O phase diagram with stability fields of hydrous phases [4, 5] and *P-T* parameters of experiments *P-T* (*a*). Schematic cross section of a slab with stability limits for antigorite and chlorite in peridotite, after [14] (*b*). Moho for hot (h.s.) and cold (c.s.) slabs is according to [15]. Blue and red arrows show flow directions of aqueous fluid and magma, respectively
NAM – nominally anhydrous minerals

This is an open access article under the CC BY 4.0 license

In the present study by performing experiments at *P-T* conditions characteristic of intermediate (warm) and hot subduction we addressed the patterns of olivine hydration by an aqueous fluid releasing from dehydrating antigorite, the effect of olivine recrystallization on its water content, and the effect of redox conditions and fluid salinity on water solubility in olivine.

Methods

Four hermetically sealed Au capsules were placed into the low-gradient zone of the high-pressure cell of the BARS multi-anvil apparatus (Fig.2). The capsules had a diameter of 2.0 mm and a wall thickness of 0.2 mm. The capsules were loaded with serpentine (Polar Urals) and specially prepared, axis-oriented polished prisms cut from olivine crystals. The serpentine used in the experiments has the following composition, wt.%: 42.6 SiO_2, 0.3 Al_2O_3, 1.6 FeO, 39.5 MgO, 0.2 CaO. The calcium impurity results from the presence of extremely thin calcite veinlets within the serpentine. A weighed portion of approximately 15 mg of serpentine was used for capsule assembly (see Table). Olivine prisms weighing from 1 to 2 mg were placed at the bottom of the capsules. In an additional series of experiments, 0.2 mg of NaCl was introduced into the serpentine samples. Two types of material were used to fabricate the prisms: the first was water-free olivine with Mg# 93 from a spinel peridotite xenolith from the "Udachnaya" kimberlite pipe; the second was olivine containing approximately 70 ppm H_2O, with Mg# 91 from a garnet peridotite xenolith from the "Udachnaya" kimberlite pipe (sample UV-419/09) [21]. During capsule assembly, all components of the system were weighed. Capsules prepared for the experiments were hermetically sealed using high-frequency arc welding with a Lampert PUK 4U device. According to the authors' estimates, the oxygen fugacity (fO_2) in the samples was close to the values of the Ni-NiO (NNO) buffer. To determine the influence of fO_2 on the concentration of OH defects in olivine, one experiment was performed using the Fe_2O_3-Fe_3O_4 (HM) buffer. Experiments lasting from 60 to 150 h were conducted on a "split-sphere" type multi-anvil apparatus at a pressure of 5.5 GPa and temperatures of 850, 940, 1030, and 1100 °C. Pressure and temperature were measured with an accuracy of ±0.1 GPa and ±20 °C, respectively.

The run products were analyzed on a Tescan MIRA 3 LMU scanning electron microscope equipped with an INCA EDS 450 microanalysis system and an Oxford Instruments EDS X-Max-80 Silicon Drift Detector. The operating conditions were: 20 kV accelerating voltage, 1 nA beam current, 3-10 μm beam diameter, and 20 s count time.

The type of OH defects and the H_2O concentration in olivine were determined using Fourier transform infrared (FTIR) spectroscopy. IR absorption spectra were measured using a Bruker Vertex 70 spectrometer equipped with a Hyperion 2000 microscope. Measurements were conducted with a resolution of 2 cm^{-1} and averaging over 64 scans. The aperture size was 30-60 μm. When analyzing the measured absorption spectra, baseline correction was performed using several methods, including linear and polynomial fitting. The uncertainty in determining the integral absorption was 15-20 %. To calculate the H_2O content in olivines, extinction coefficients of 0.119 and 0.055 wt. ppm H_2O cm^{-2} were used for the high-frequency (3650-3350 cm^{-1}) [22, 23] and low-frequency (3350-3000 cm^{-1}) [24] regions of the OH absorption spectra, respectively.

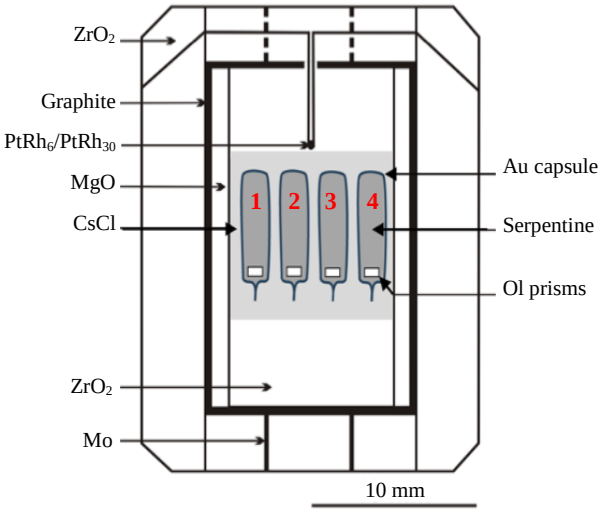


Fig.2. High-pressure cell with assembled Au capsules (1-4). Located in a low-gradient zone (gray rectangular)

$PtRh_6/PtRh_{30}$ – thermocouple used for temperature monitoring

This is an open access article under the CC BY 4.0 license

Journal of Mining Institute. 2026. Vol. 279. P. 3-12
© Igor N. Kupriyanov, Aleksandr G. Sokol, 2026

Starting compositions, parameters of experiments at P = 5.5 GPa and phase compositions of run products

Run number	Starting composition				Buffer	T, °C	Time, h	H_2O^*, wt.%	Phase composition
	Serpentine, mg	Olivine		NaCl, mg					
		Type	Weight, mg						
2304_2_3	11.9	–	–	–	–	850	150	16	Ol, Opx, Fl
2304_2_4	12.0	Ol(dry)**	5.8	–	–	850	150	9	Ol, Opx, Fl
2306_2_1	12.0	Ol(dry)	5.0	–	–	940	240	n.d.	Ol, Opx, Fl
855_6_3	13.8	Ol(dry) + Ol(H_2O)	1.3 + 1.9	–	–	850	90	11	Ol, Opx, Fl
2332_2_3	11.8	Ol(dry) + Ol(H_2O)	1.2 + 1.5	–	–	1030	90	9	Ol, Opx, Fl
845_8_1	12.5	–	–	–	–	1030	90	12	Ol, Opx, Fl
872_6_1	14.2	Ol(H_2O)***	1.4	–	–	1100	60	n.d.	Ol, Opx, Fl
872_6_4	13.9	Ol(dry)	2.7	–	–	1100	60	n.d.	Ol, Opx, Fl
845_8_2	12.1	–	–	–	HM	1030	90	12	Ol, Opx, Fl
1772_3_5	15.0	–	–	0.2	–	850	100	11	Ol, Opx, Fl
1400_4_6	15.0	–	–	0.2	–	1030	100	12	Ol, Opx, Fl

* Amount of H_2O released upon opening of Au capsules after the experiments, normalized to the sample mass.
** Water-free olivine from a spinel peridotite xenolith from the "Udachnaya" kimberlite pipe.
*** Olivine containing approximately 70 ppm H_2O, from a garnet peridotite xenolith from the "Udachnaya" kimberlite pipe (UV-419/09) [21]; Ol – olivine; Opx – orthopyroxene; Fl – fluid; n.d. – not determined.

Results and discussion

Antigorite containing 13 wt.% H_2O breaks down with formation of olivine, orthopyroxene, and a supercritical aqueous fluid. Experiments carried out 5.5 GPa and 850 °C for 90 to 150 h yielded an aggregate of ≤ 15 μm irregularly shaped olivine and orthopyroxene grains surrounded by acicular and dendritic quench phases of the aqueous fluid with variable SiO_2 and MgO contents (Fig.3, *a*). Newly formed olivine contained 4.1 wt.% FeO. Orthopyroxene contained 3.2 wt.% FeO, 0.8 wt.% Al_2O_3, and 0.3 wt.% CaO. Some olivine prisms cracked upon pressure increase while others remained intact. Olivine itself retained its mineral chemistry after the runs, but a ≤ 10 μm layer of newly formed olivine with 4.2-4.4 wt.% FeO appeared on the prism surface. The phases produced in the experiment at 940 °C for 90 h had compositions almost the same as those from runs at 850 °C.

With an increase in temperature to 1030 °C at the same experimental duration, the FeO content in olivine produced through serpentine dehydration increased to 4.6 wt.%. Orthopyroxene associated with olivine contained 2.8 wt.% FeO, 0.5 wt.% Al_2O_3, and 0.4 wt.% CaO. The prisms that retained their integrity, as well as their fragments, exhibit a layer of newly formed olivine up to 20 μm thick on their surfaces after the experiments (Fig.3, *b*). Its composition corresponds to that of the fine-grained olivine from the serpentine dehydration products. In the sample obtained from the experiment

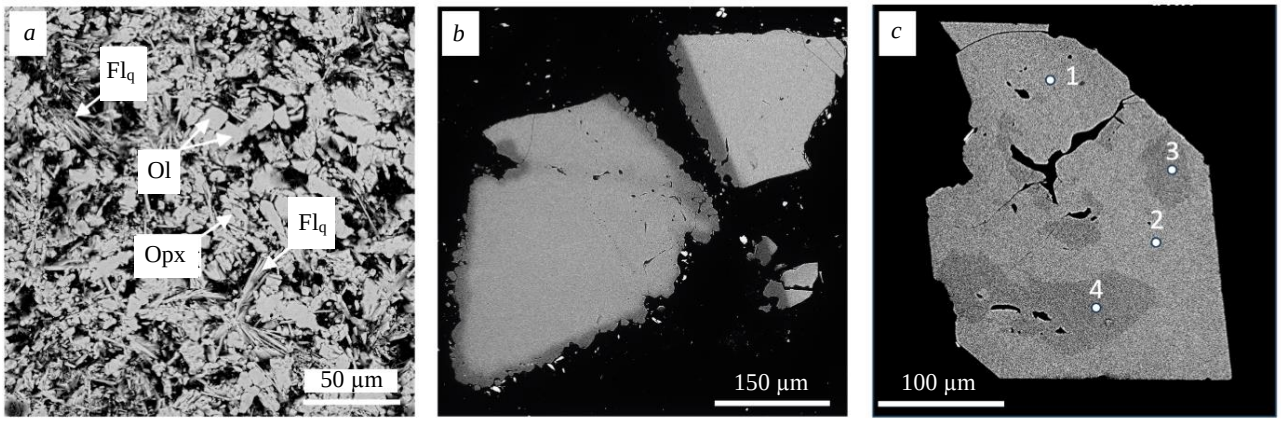


Fig.3. An aggregate Ol and Opx grains and aqueous fluid quench products from experiment 855_6_3 (850 °C) (*a*).
Fragments of starting olivine prisms after experiment 2332_2_3 (1030 °C) (*b*).
A fragment of water-free olivine prism with internal regions of recrystallization (experiment 872_6_4, 1100 °C) (*c*)
1-4 – areas of FTIR spectra measurements

This is an open access article under the CC BY 4.0 license

at 1100 °C, the compositions of olivine and orthopyroxene remained the same as at 1030 °C. However, extensive zones of olivine recrystallization were recorded within the prisms, traced by a reduced FeO content (Fig.3, *c*). The arrangement of inclusion chains within these zones suggests that recrystallization occurred along fractures. The fractures could have formed during the initial stage of the experiment upon pressure increase and then partially healed when the target *P-T* parameters were reached.

Plane-parallel plates with a thickness of 200-300 μm were prepared from the olivine prisms extracted from the capsules after the experiments, and these were studied using FTIR spectroscopy. Let us consider the results obtained for each type of the starting olivine. As follows from the FTIR spectra presented in Fig.4, the predominant type of OH defects in the initial water-bearing olivine from garnet peridotite consists of protonated silicon vacancies (V_{Si} + $4H^+$, hereinafter referred to as [Si]-OH), which are manifested in the spectra by a series of absorption peaks with maxima at 3613, 3580, 3567, and 3550 cm^{-1} [24-26]. The weak peaks in the 3400-3300 cm^{-1} range, which are also present in the spectra of the initial olivine, correspond to OH defects associated with trivalent cations Fe^{3+}, Al^{3+}, Cr^{3+} [27, 28]. According to the authors' calculations, the water concentration in the initial olivine is 70 ppm. The FTIR spectra measured after the experiments are presented in Fig.5. For the water-bearing olivine, it was established that the intensity of the absorption bands associated with protonated Si vacancies increases noticeably after the experiments, while the magnitude of this increase is practically independent of temperature. The authors estimate that the H_2O concentrations in olivine after the experiments at 850 and 1030 °C amount to 110 and 120 ppm, respectively. The overall appearance of the spectra in the OH region remains virtually unchanged. The spectra are dominated by bands of [Si]-OH defects, the relative intensity of the weak bands in the 3400-3300 cm^{-1} region changes slightly, and absorption bands associated with OH defects at magnesium vacancies (3300-3000 cm^{-1}) are not detected.

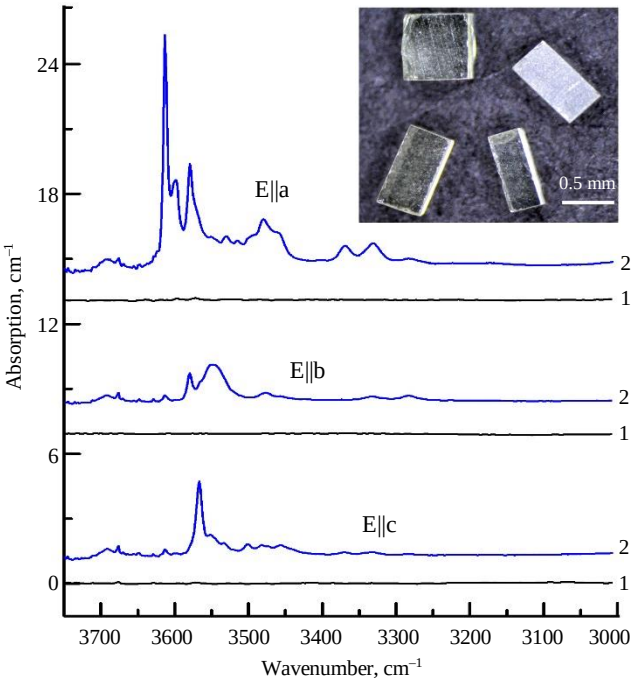


Fig.4. Polarized FTIR spectra recorded for initial water-free olivine from spinel peridotite (1) and water-bearing olivine from garnet peridotite (2) xenoliths from "Udachnaya" kimberlite pipe. The spectra are shifted along the vertical axis for clarity. Inset shows prepared oriented olivine prisms

A different behavior pattern of OH defects was established for the water-free olivine from spinel peridotite (Fig.5, *b*). After the experiment at 850 °C, only a weak, relatively broad band with a maximum near 3190 cm^{-1} was recorded in the IR spectrum of the olivine. According to generally accepted concepts, this band is associated with OH defects at magnesium vacancies (V_{Mg} + $2H^+$, hereinafter referred to as [Mg]-OH) [24, 25, 29]. After the experiment at T = 1030 °C, the intensity of this band increased substantially, whereas the intensity of the bands attributed to [Si]-OH defects barely exceeds the noise level. The authors estimate that in this case, the H_2O concentrations after the experiments at 850 and 1030 °C amount to 3 and 17 ppm, respectively. The study of oriented plates prepared after the experiments showed that for both types of initial olivine, the distribution of OH defects within them is homogeneous, provided that the samples do not exhibit internal structural features associated with olivine recrystallization during the experiments.

This is an open access article under the CC BY 4.0 license

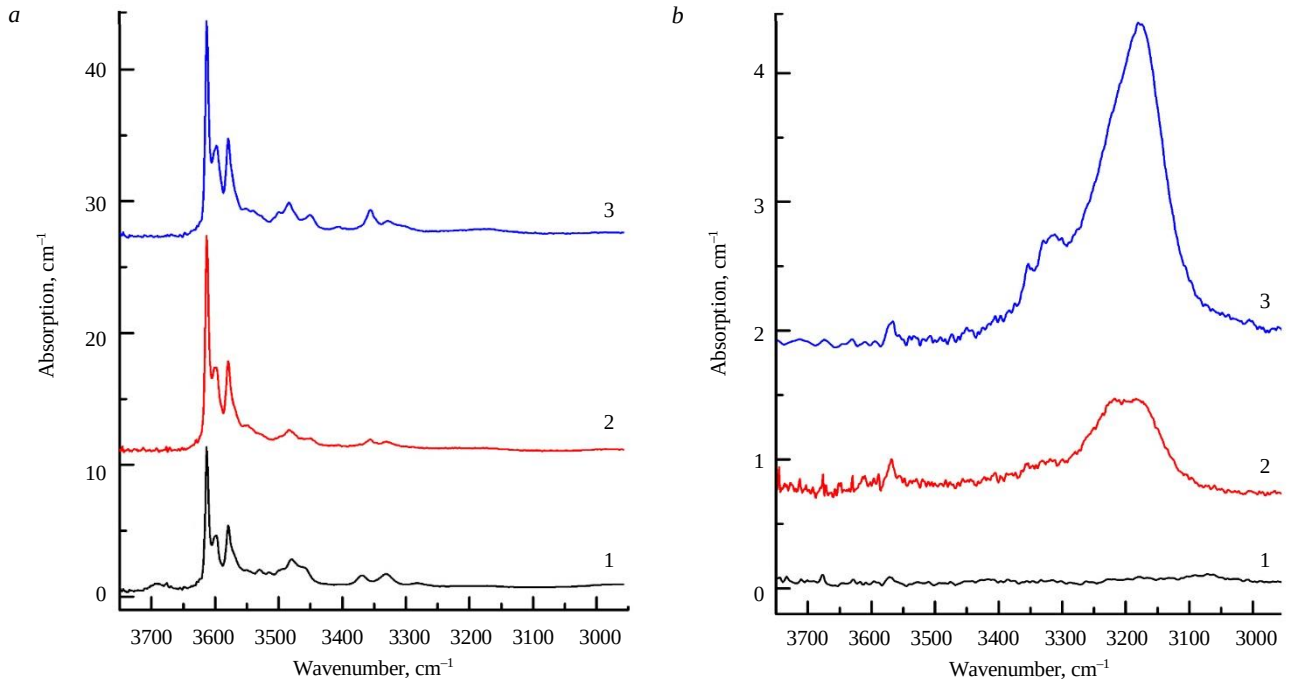


Fig.5. FTIR spectra, recorded for water-bearing (*a*) and water-free (*b*) olivine before (1) and after experiments at 850 °C (2) and 1030 °C (3)

Figure 6 shows the averaged unpolarized FTIR spectra measured for crystallites of newly formed olivine from experiments at temperatures of 940, 1030, and 1100 °C. The grain size of olivine formed in the experiment at T = 850 °C did not exceed 20 μm, which is insufficient for IR measurements. As seen in Fig.6, the intensity of the OH defect bands increases continuously with increasing temperature. According to the authors' estimates, the H_2O concentration in olivine formed at T = 940 °C is 140 ppm, increasing to 230 ppm at T = 1030 °C, and reaching 350 ppm at T = 1100 °C. In the latter case, the FTIR spectra exhibit absorption bands of both [Si]-OH and [Mg]-OH defects, whereas in the spectra of olivines obtained at lower temperatures, [Si]-OH defects predominate. The introduction of an NaCl additive into the serpentine ensured the presence of 9 wt.% NaCl in the aqueous fluid, i.e., at a level characteristic of dehydration fluids in subduction zones [30]. Data obtained from experiments at 850 and 1030 °C indicate that such chloride content in the aqueous fluid has either no effect or only a minimal effect on the water concentration in the newly formed olivine. In the experiment at 1030 °C, the influence of highly oxidizing conditions, controlled by the HM buffer, on the fractionation of water between the aqueous fluid and newly formed olivine was studied. According to the data obtained, an increase in fO_2 from the NNO buffer values (characteristic of the majority of experiments) to the HM buffer values had no detectable effect on the water content in the newly formed olivine.

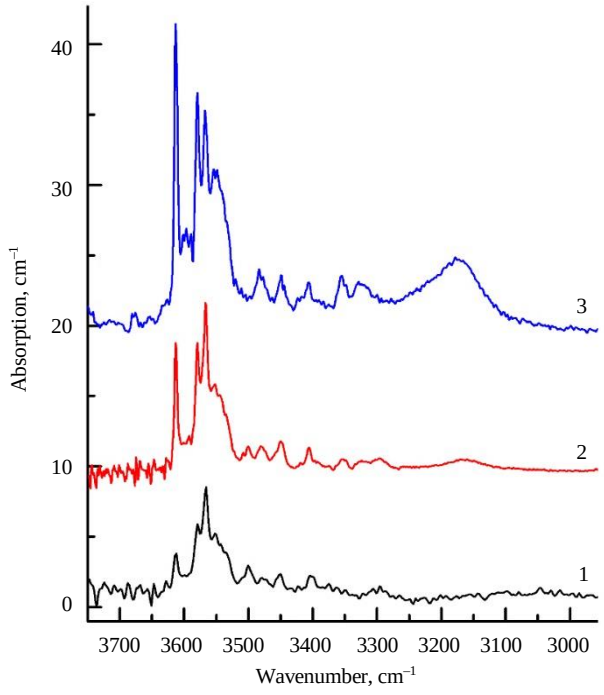


Fig.6. FTIR spectra of newly formed olivine produced in experiments at 940 °C (1), 1030 °C (2), and 1100 °C (3)

This is an open access article under the CC BY 4.0 license

It was noted that in the experiment at 1100 °C, extensive recrystallization zones traced by a reduced FeO content were recorded within the olivine prisms. Figure 7 presents the FTIR spectra measured in various regions of the water-free olivine sample containing internal recrystallization domains (see Fig.3, *c*). As seen in Fig.7, the distribution of OH defects in this case is heterogeneous. The intensity of the OH bands and, consequently, the concentration of OH defects are significantly higher in the regions that underwent recrystallization processes.

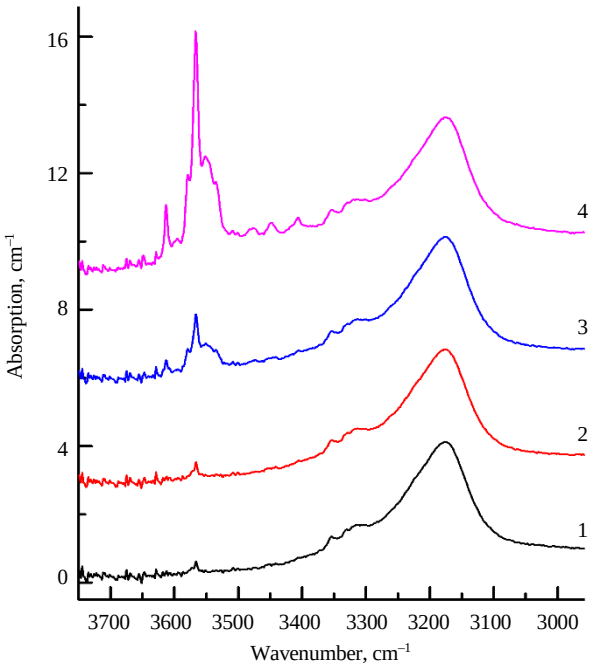


Fig.7. FTIR spectra recorded from different areas of a fragment of water-free olivine prism with recrystallization zones (T = 1100 °C). The spectra are numbered according to numbers of the areas marked in Fig.3, *c*

Analysis of the obtained data led to the conclusion that upon reaching a pressure of 5.5 GPa and temperatures of 850, 940, 1030, and 1100 °C, the serpentine underwent dehydration, during which a phase assemblage of olivine, orthopyroxene, and an aqueous fluid was formed. During the prolonged experiments, the aqueous fluid dissolved silicate components and thereby achieved equilibrium with the olivine and orthopyroxene. The formation of layers of newly formed olivine on the surface of the olivine prisms provides direct evidence of this. In this case, the activity of silica in the fluid was controlled by olivine and orthopyroxene at a level characteristic of peridotites. This is principally important, since the concentration of silicon and magnesium vacancies in the newly formed olivine depends on the silica activity in crystallization environment [31]. The concentration of vacancies in olivine from subducting peridotite, the genesis of which is not related to serpentine dehydration, is determined by the specific features of its crystallization in environments outside subduction zones.

The interaction of the aqueous fluid with olivine at *P-T* parameters characteristic of subduction zones is largely controlled by the defectiveness of the olivine crystal structure, primarily by the concentration of pre-existing silicon vacancies. According to the data obtained, at a temperature of 850 °C, pre-existing silicon vacancies in the olivine undergo protonation and the concentration of [Si]-OH defects increases noticeably relative to the initial value. As the temperature increases to 1030 °C, no new silicon vacancies are generated, and the concentration of [Si]-OH defects remains virtually unchanged compared to experiments at lower temperatures. The concentration of OH defects at magnesium vacancies increases with increasing temperature; however, the contribution of this mechanism to the total concentration of OH defects is extremely small, not exceeding 20 ppm at temperatures of ~1000 °C. The formation of new silicon vacancies and their protonation during the recrystallization of olivine in an aqueous fluid is established only at 1100 °C, near the solidus of the peridotite-H_2O system [31]. This mechanism provides the largest contribution to the increase in water solubility in olivine and is realized only at temperatures characteristic of the mantle wedge.

It is known that the solubility of water in nominally anhydrous minerals is significantly influenced by redox conditions [32, 33], water activity in the crystallization medium [18, 31, 34], as well as the composition of the growth medium [31, 35-37]. According to data from [38], serpentine dehydration causes an increase in fO_2 in subducting peridotites to values practically close to the HM buffer. The data obtained in the present study indicate that such a change in redox conditions has little or no effect on the solubility of water in olivine. It has been noted that dehydration fluids in subduction zones contain NaCl at levels of up to 10 wt.% [30]. At mantle *P-T* parameters, NaCl significantly reduces the solubility of SiO_2 in aqueous fluid [39], which should increase water activity in the olivine crystallization medium. However, the authors' data indicate that NaCl concentrations characteristic of

This is an open access article under the CC BY 4.0 license

dehydration fluids in subduction zones have no, or only minor, effect on the water concentration in newly formed olivine.

Analysis of the obtained data shows that they do not agree with the model of subsolidus water solubility in olivine proposed in [18]. The model is based on experimental data on olivine hydrogenation obtained at a fixed pressure of 3 GPa and temperatures ranging from 750-1050 °C, and at a fixed temperature of 950 °C with pressures ranging from 0.5-6 GPa. The initial olivines contained titanium impurities, which led to a significant contribution from Ti-clinohumite-like point defects (Ti-OH defects) to the total H_2O content. The model allows for the calculation of the maximum water content in olivine for the thermal conditions characteristic of subduction zones, as well as for the assessment of the mantle wedge's potential as a water transporter into the mantle. According to the model, the maximum water concentration in olivine at 5.5 GPa and 850 °C (characteristic of the mantle wedge at a distance of 1.5 km from the surface of a cold slab [1]) is 400 ppm. Meanwhile, at a temperature of 1100 °C (characteristic of the mantle wedge at a distance of 5.5 km from the surface of a cold slab), the concentration according to the model [18] could reach 900 ppm. The results obtained in the present study suggest that these values are substantially overestimated. In the presence of an aqueous fluid in equilibrium with peridotite at a pressure of 5.5 GPa and a temperature of 940 °C, the water concentration in newly formed olivine does not exceed 140 ppm, and in olivine that has not undergone recrystallization, it does not exceed 110 ppm. With an increase in temperature to 1030 °C, the water concentration in newly formed olivine reaches only 230 ppm, while in peridotitic olivine with its pre-existing suite of silicon vacancies, it remains practically unchanged at around 120 ppm.

With a further increase in pressure in the subducting slab, the solubility of water in olivine may increase substantially [31, 35, 36]. This is attributed to the fact that the activity of silica in an aqueous fluid in equilibrium with peridotite can decrease significantly. According to researchers [36], this is evidenced by the predominance of Si vacancies over Mg vacancies in olivine synthesized at $P \geq 8$ GPa. Already at a pressure of 12 GPa, the activity of silica in the crystallization medium exerts a secondary influence on water solubility, which reaches 8900 ppm at 1250 °C [35].

An analysis of the data obtained in the present study, taking into account the weak dependence of water solubility in olivine on pressure in the 4-6 GPa range at subduction temperatures [18], leads to the conclusion that the efficiency of water transport into the mantle by nominally anhydrous minerals, and primarily by olivine, is minimal precisely at depths of ~150-200 km, immediately after the complete dehydration of serpentine in the slab. In the mantle wedge, the breakdown of serpentine occurs much earlier, at $P < 3$ GPa [1]. The low concentration of H_2O in olivine in the form of OH defects established at a pressure of 5.5 GPa indicates an insignificant role for lithospheric mantle peridotites and the portions of the mantle wedge mechanically coupled to the slab in transporting water to depths greater than 150 km under intermediate (warm) and hot subduction regimes. According to the authors of [4], the characteristics of thermal regimes and the features of alkali fractionation in subduction zones indicate that the efficiency of amphibole and phengite as water transporters to depths greater than 120 km is low. At the same time, recent experimental data show that the role of chlorite and lawsonite in this process may remain underestimated [8, 40]. Under these conditions, a possibility arises for the release and ascent of aqueous fluid into magma generation regions. Since fluids in subduction zones migrate subvertically, in steeply dipping ($\geq 60°$) slabs such as those at Marianas, New Britain, Solomon, and Vanuatu, the dehydration fluids generated at depths of 130-200 km (corresponding to 4-6 GPa) can directly enter the regions of island-arc magma generation [41]. Furthermore, as aqueous fluids migrate into the mantle, they can participate in mineral formation processes, including diamond formation [42-44].

Conclusion

Analysis of the obtained experimental data led to the conclusion that the efficiency of water transport into the mantle by nominally anhydrous minerals, primarily olivine, is minimal precisely at depths of ~150-200 km, immediately after the complete dehydration of serpentine in slabs subducting under the thermal regimes of warm and hot subduction. This is attributed to the fact that under such

This is an open access article under the CC BY 4.0 license

conditions, the interaction of the dehydration aqueous fluid with olivine is largely controlled by the defectiveness of the olivine crystal structure, primarily by the presence of silicon vacancies. At a pressure of 5.5 GPa and a temperature of 850 °C, pre-existing silicon vacancies in the olivine undergo protonation; in this case, the concentration of [Si]-OH defects increases noticeably relative to the initial value, but the water content remains at a level of 110 ppm. With an increase in temperature to 1030 °C, new silicon vacancies do not form, and the concentration of [Si]-OH defects remains at the same level as during hydrogenation at lower temperatures. The concentration of OH defects related to magnesium vacancies increases with increasing temperature; however, the contribution of this mechanism to the total concentration of OH defects is extremely small. The generation of new silicon vacancies during the recrystallization of olivine in an aqueous fluid near the peridotite solidus makes the largest contribution to the increase in water solubility. However, even in this case, the water content in the newly formed olivine reaches only 350 ppm.

The authors express their sincere gratitude to Yu.M.Borzdov, Yu.N.Palyanov and A.F.Khokhryakov for their valuable comments, which helped to improve the presentation of the material. Analytical studies were conducted at the Analytical Center for multi-elemental and isotope research SB RAS.

REFERENCES

1. van Keken P.E., Hacker B.R., Syracuse E.M., Abers G.A. Subduction factory: 4. Depth-dependent flux of H2O from subducting slabs worldwide. *Journal of Geophysical Research: Solid Earth*. 2011. Vol. 116. Iss. B1. N B01401. DOI: 10.1029/2010JB007922

2. Hirschmann M.M. Comparative deep Earth volatile cycles: The case for C recycling from exosphere/mantle fractionation of major (H_2O, C, N) volatiles and from H_2O/Ce, CO_2/Ba, and CO_2/Nb exosphere ratios. *Earth and Planetary Science Letters*. 2018. Vol. 502, p. 262-273. DOI: 10.1016/j.epsl.2018.08.023

3. Ohtani E. Hydration and Dehydration in Earth's Interior. *Annual Review of Earth and Planetary Sciences*. 2021. Vol. 49, p. 253-278. DOI: 10.1146/annurev-earth-080320-062509

4. Keppler H., Ohtani E., Xiaozhi Yang. The Subduction of Hydrogen: Deep Water Cycling, Induced Seismicity, and Plate Tectonics. *Elements*. 2024. Vol. 20. N 4, p. 229-234. DOI: 10.2138/gselements.20.4.229

5. Schmidt M.W., Poli S. Devolatilization During Subduction. *Treatise on Geochemistry. Elsevier*, 2014. Vol. 4, p. 669-701. DOI: 10.1016/B978-0-08-095975-7.00321-1

6. Grevemeyer I., Ranero C.R., Ivandic M. Structure of oceanic crust and serpentinization at subduction trenches. *Geosphere*. 2018. Vol. 14. N 2, p. 395-418. DOI: 10.1130/GES01537.1

7. Chen Cai, Wiens D.A., Weisen Shen, Eimer M. Water input into the Mariana subduction zone estimated from ocean-bottom seismic data. *Nature*. 2018. Vol. 563, p. 389-392. DOI: 10.1038/s41586-018-0655-4

8. Hermann J., Lakey S. Water transfer to the deep mantle through hydrous, Al-rich silicates in subduction zones. *Geology*. 2021. Vol. 49. № 8. P. 911-915. DOI: 10.1130/G48658.1

9. Fumagalli P., Stixrude L., Poli S., Snyder D. The 10Å phase: a high-pressure expandable sheet silicate stable during subduction of hydrated lithosphere. *Earth and Planetary Science Letters*. 2001. Vol. 186. Iss. 2, p. 125-141. DOI: 10.1016/S0012-821X(01)00238-2

10. Inoue T., Wada T., Sasaki R., Yurimoto H. Water partitioning in the Earth's mantle. *Physics of the Earth and Planetary Interiors*. 2010. Vol. 183. Iss. 1-2, p. 245-251. DOI: 10.1016/j.pepi.2010.08.003

11. Sobolev A.V., Asafov E.V., Gurenko A.A. et al. Komatiites reveal a hydrous Archaean deep-mantle reservoir. *Nature*. 2016. Vol. 531. Iss. 7596, p. 628-632. DOI: 10.1038/nature17152

12. Harte B., Harris J.W., Hutchison M.T. et al. Lower mantle mineral associations in diamonds from Sao Luiz, Brazil. *Mantle petrology: Field Observations and High-pressure Experimentation* (*A Tribute to Francis R.* (*Joe*) *Boyd*). 1999. Vol. 6, p. 125-153.

13. Pearson D.G., Canil D., Shirey S.B. Mantle Samples Included in Volcanic Rocks: Xenoliths and Diamonds. *Treatise on Geochemistry. Elsevier*, 2003. Vol. 2, p. 171-275. DOI: 10.1016/B0-08-043751-6/02005-3

14. Flemetakis S., Tiraboschi C., Rohrbach A. et al. The stability of antigorite in subduction zones revisited: the effect of F on antigorite stability and its breakdown reactions at high pressures and high temperatures, with implications for the geochemical cycles of halogens. *Contributions to Mineralogy and Petrology*. 2022. Vol. 177. Iss. 7. N 70. DOI: 10.1007/s00410-022-01934-5

15. Syracuse E.M., van Keken P.E., Abers G.A. The global range of subduction zone thermal models. *Physics of the Earth and Planetary Interiors*. 2010. Vol. 183. Iss. 1-2, p. 73-90. DOI: 10.1016/j.pepi.2010.02.004

16. Ferrand T.P. Neither antigorite nor its dehydration is "metastable". *American Mineralogist*. 2019. Vol. 104. Iss. 6, p. 788-790. DOI: 10.1016/j.pepi.2010.02.004

17. Maurice J., Bolfan-Casanova N., Demouchy S. et al. The intrinsic nature of antigorite breakdown at 3 GPa: Experimental constraints on redox conditions of serpentinite dehydration in subduction zones. *Contributions to Mineralogy and Petrology*. 2020. Vol. 175. Iss. 10. N 94. DOI: 10.1007/s00410-020-01731-y

18. Padrón-Navarta J.A., Hermann J. A Subsolidus Olivine Water Solubility Equation for the Earth's Upper Mantle. *Journal of Geophysical Research: Solid Earth*. 2017. Vol. 122. Iss. 12, p. 9862-9880. DOI: 10.1002/2017JB014510

19. Mierdel K., Keppler H., Smyth J.R., Langenhorst F. Water Solubility in Aluminous Orthopyroxene and the Origin of Earth's Asthenosphere. *Science*. 2007. Vol. 315. Iss. 5810, p. 364-368. DOI: 10.1126/science.1135422

This is an open access article under the CC BY 4.0 license

20. Férot A., Bolfan-Casanova N. Water storage capacity in olivine and pyroxene to 14 GPa: Implications for the water content of the Earth's upper mantle and nature of seismic discontinuities. *Earth and Planetary Science Letters*. 2012. Vol. 349-350, p. 218-230. DOI: 10.1016/j.epsl.2012.06.022

21. Doucet L.S., Ionov D.A., Golovin A.V. The origin of coarse garnet peridotites in cratonic lithosphere: new data on xenoliths from the Udachnaya kimberlite, central Siberia. *Contributions to Mineralogy and Petrology*. 2013. Vol. 165. Iss. 6, p. 1225-1242. DOI: 10.1007/s00410-013-0855-8

22. Withers A.C., Bureau H., Raepsaet C., Hirschmann M.M. Calibration of infrared spectroscopy by elastic recoil detection analysis of H in synthetic olivine. *Chemical Geology*. 2012. Vol. 334, p. 92-98. DOI: 10.1016/j.chemgeo.2012.10.002

23. Towbin W.H., Plank T., Klein E., Hauri E. Measuring H_2O concentrations in olivine by secondary ion mass spectrometry: Challenges and paths forward. *American Mineralogist*. 2023. Vol. 108. Iss. 5, p. 928-940. DOI: 10.2138/am-2022-8247

24. Kovács I., O'Neill H.St.C., Hermann J., Hauri E.H. Site-specific infrared O-H absorption coefficients for water substitution into olivine. *American Mineralogist*. 2010. Vol. 95. Iss. 2-3, p. 292-299. DOI: 10.2138/am.2010.3313

25. Berry A.J., Hermann J., O'Neill H.S.C., Foran G.J. Fingerprinting the water site in mantle olivine. *Geology*. 2005. Vol. 33. N 11, p. 869-872. DOI: 10.1130/G21759.1

26. Xianyu Xue, Kanzaki M., Turner D., Loroch D. Hydrogen incorporation mechanisms in forsterite: New insights from ^{1}H and ^{29}Si NMR spectroscopy and first-principles calculation. *American Mineralogist*. 2017. Vol. 102. Iss. 3, p. 519-536. DOI: 10.2138/am-2017-5878

27. Berry A.J., O'Neill H.St.C., Hermann J., Scott D.R. The infrared signature of water associated with trivalent cations in olivine. *Earth and Planetary Science Letters*. 2007. Vol. 261. Iss. 1-2, p. 134-142. DOI: 10.1016/j.epsl.2007.06.021

28. Blanchard M., Ingrin J., Balan E. et al. Effect of iron and trivalent cations on OH defects in olivine. *American Mineralogist*. 2017. Vol. 102. Iss. 2, p. 302-311. DOI: 10.2138/am-2017-5777

29. Crépisson C., Bureau H., Blanchard M. et al. Theoretical infrared spectrum of partially protonated cationic vacancies in forsterite. *European Journal of Mineralogy*. 2014. Vol. 26. N 2, p. 203-210. DOI: 10.1127/0935-1221/2014/0026-2366

30. Manning C.E., Frezzotti M.L. Subduction-Zone Fluids. *Elements*. 2020. Vol. 16. N 6, p. 395-400. DOI: 10.2138/gselements.16.6.395

31. Bali E., Bolfan-Casanova N., Koga K.T. Pressure and temperature dependence of H solubility in forsterite: An implication to water activity in the Earth interior. *Earth and Planetary Science Letters*. 2008. Vol. 268. Iss. 3-4, p. 354-363. DOI: 10.1016/j.epsl.2008.01.035

32. Sokol A.G., Palyanov Y.N., Kupriyanov I.N. et al. Effect of oxygen fugacity on the H_2O storage capacity of forsterite in the carbon-saturated systems. *Geochimica et Cosmochimica Acta*. 2010. Vol. 74. Iss. 16, p. 4793-4806. DOI: 10.1016/j.gca.2010.05.032

33. Bolfan-Casanova N., Martinek L., Manthilake G. et al. Effect of oxygen fugacity on the storage of water in wadsleyite and olivine in H and H-C fluids and implications for melting atop the transition zone. *European Journal of Mineralogy*. 2023. Vol. 35. Iss. 4, p. 549-568. DOI: 10.5194/ejm-35-549-2023

34. Sokol A.G., Kupriyanov I.N., Palyanov Y.N. Partitioning of H_2O between olivine and carbonate–silicate melts at 6.3 GPa and 1400 °C: Implications for kimberlite formation. *Earth and Planetary Science Letters*. 2013. Vol. 383, p. 58-67. DOI: 10.1016/j.epsl.2013.09.030

35. Smyth J.R., Frost D.J., Nestola F. et al. Olivine hydration in the deep upper mantle: Effects of temperature and silica activity. *Geophysical Research Letters*. 2006. Vol. 33. Iss. 15. N L15301. DOI: 10.1029/2006GL026194

36. Withers A.C., Hirschmann M.M. Influence of temperature, composition, silica activity and oxygen fugacity on the H_2O storage capacity of olivine at 8 GPa. *Contributions to Mineralogy and Petrology*. 2008. Vol. 156. Iss. 5, p. 595-605. DOI: 10.1007/s00410-008-0303-3

37. Sokol A.G., Kupriyanov I.N., Palyanov Y.N. et al. Melting experiments on the Udachnaya kimberlite at 6.3-7.5 GPa: Implications for the role of H_2O in magma generation and formation of hydrous olivine. *Geochimica et Cosmochimica Acta*. 2013. Vol. 101, p. 133-155. DOI: 10.1016/j.gca.2012.10.018

38. Cannaò E., Malaspina N. From oceanic to continental subduction: Implications for the geochemical and redox evolution of the supra-subduction mantle. *Geosphere*. 2018. Vol. 14. N 6, p. 2311-2336. DOI: 10.1130/GES01597.1

39. Rustioni G., Audetat A., Keppler H. The composition of subduction zone fluids and the origin of the trace element enrichment in arc magmas. *Contributions to Mineralogy and Petrology*. 2021. Vol. 176. Iss. 7. N 51. DOI: 10.1007/s00410-021-01810-8

40. Hernández-Uribe D., Tsujimori T. Progressive lawsonite eclogitization of the oceanic crust: Implications for deep mass transfer in subduction zones. *Geology*. 2023. Vol. 51. N 7, p. 678-682. DOI: 10.1130/G51052.1

41. Schmidt M.W., Jagoutz O. The global systematics of primitive arc melts. *Geochemistry, Geophysics, Geosystems*. 2017. Vol. 18. Iss. 8, p. 2817-2854. DOI: 10.1002/2016GC006699

42. Luth R.W., Palyanov Y.N., Bureau H. Experimental Petrology Applied to Natural Diamond Growth. *Reviews in Mineralogy and Geochemistry*. 2022. Vol. 88. N 1, p. 755-808. DOI: 10.2138/rmg.2022.88.14

43. Simakov S.K., Stegnitskiy Yu.B. On the presence of the postmagmatic stage of diamond formation in kimberlites. *Journal of Mining Institute*. 2022. Vol. 255, p. 319-326. DOI: 10.31897/PMI.2022.22

44. Gubanov N.V., Zedgenizov D.A., Vasilev E.A., Naumov V.A. New data on the composition of growth medium of fibrous diamonds from the placers of the Western Urals. *Journal of Mining Institute*. 2023. Vol. 263, p. 645-656.

***Authors*: Igor N. Kupriyanov,** *Senior Researcher* (*V.S.Sobolev Institute of Geology and Mineralogy SB RAS, Novosibirsk, Russia*), *spectra@igm.nsc.ru, https://orcid.org/0000-0002-3326-0939*, **Aleksandr G. Sokol,** *Doctor of Geological and Mineralogical Sciences, Chief Researcher* (*V.S.Sobolev Institute of Geology and Mineralogy SB RAS, Novosibirsk, Russia*), *https://orcid.org/0000-0002-7721-5152*.

The authors declare no conflict of interests.

This is an open access article under the CC BY 4.0 license